

# Constraints on the dark matter annihilation from Fermi-LAT observation of M31

Zhengwei Li<sup>a,b</sup>, Xiaoyuan Huang<sup>c</sup>, Qiang Yuan<sup>a1</sup>, and Yupeng Xu<sup>b</sup>

<sup>a</sup>Key Laboratory of Dark Matter and Space Astronomy, Purple Mountain Observatory, Chinese Academy of Sciences, Nanjing 210008, P.R.China

<sup>b</sup>Key Laboratory of Particle Astrophysics, Institute of High Energy Physics, Chinese Academy of Sciences, Beijing 100049, P.R. China

<sup>c</sup>Physik-Department T30d, Technische Universität München, James-Franck-Straße, D-85748 Garching, Germany

E-mail: [lizw@ihep.ac.cn](mailto:lizw@ihep.ac.cn), [huangxiaoyuan@gmail.com](mailto:huangxiaoyuan@gmail.com), [yuanq@pmo.ac.cn](mailto:yuanq@pmo.ac.cn), [xuyp@ihep.ac.cn](mailto:xuyp@ihep.ac.cn)

**Abstract.** Gamma-ray is a good probe of dark matter (DM) particles in the Universe. We search for the DM annihilation signals in the direction of the Andromeda galaxy (M31) using 7.5 year Fermi-LAT pass 8 data. Similar to Pshirkov et al. (2016), we find that there is residual excess emission from the direction of M31 if only the galactic disk as traced by the far infrared emission is considered. Adding a point-like source will improve the fitting effectively, although additional slight improvements can be found if an extended component such as a uniform disk or two bubbles is added instead. Taking the far infrared disk plus a point source as the background model, we search for the DM annihilation signals in the data. We find that there is strong degeneracy between the emission from the galaxy and that from 10s GeV mass DM annihilation in the main halo with quark final state. However, the required DM annihilation cross section is about  $10^{-25} - 10^{-24} \text{ cm}^3\text{s}^{-1}$ , orders of magnitude larger than the constraints from observations of dwarf spheroidal galaxies, indicating a non-DM origin of the emission. If DM subhalos are taken into account, the degeneracy is broken. When considering the enhancement from DM subhalos, the constraints on DM model parameters are comparable to (or slightly weaker than) those from the population of dwarf spheroidal galaxies. We also discuss the inverse Compton scattering component from DM annihilation induced electrons/positrons. For the first time we include an energy dependent template of the inverse Compton emission (i.e., a template cube) in the data analysis to take into account the effect of diffusion of charged particles. We find a significant improvement of the constraints in the high mass range of DM particles after considering the inverse Compton emission.

**Keywords:** dark matter, gamma ray, M31

**ArXiv ePrint:** [1312.7609](https://arxiv.org/abs/1312.7609)

---

<sup>1</sup>For correspondence.

---

## Contents

<b>1</b>	<b>Introduction</b>	<b>1</b>
<b>2</b>	<b>Gamma ray flux from DM annihilation in M31</b>	<b>2</b>
2.1	DM density profile	2
2.2	Substructures	3
<b>3</b>	<b>Data analysis</b>	<b>5</b>
<b>4</b>	<b>Constraints on DM annihilation models</b>	<b>7</b>
4.1	Prompt radiation only	7
4.2	Including ICS emission	10
<b>5</b>	<b>Conclusion and discussion</b>	<b>12</b>

---

## 1 Introduction

It has been over 80 years since the first discovery of dark matter (DM) by F. Zwicky in the 1930s [1], but the particle nature of DM remains one of the biggest unsolved problems of physics. Many astronomical observations show that the majority of DM should be made of non-baryonic, non-luminous, and cold matter. The most popular candidate is a weakly interacting massive particle (WIMP), which could just produce the right relic density of DM assuming thermal freezing out of DM particles in the early Universe. Widely discussed candidates include the lightest particle in the supersymmetric extension of the standard model (SM) or the universal extra dimension theory [2–4]. Self-annihilation or decay of WIMPs into SM particles can produce charged particles and  $\gamma$ -rays with signatures different from the ordinary astrophysical background, which may be detectable in the cosmic ray or multi-wavelength electromagnetic observations [5–7].

The Fermi Large Area Telescope (Fermi-LAT) [8], launched in 2008, is up to now the most sensitive detector for GeV  $\gamma$ -rays. It significantly improves the sensitivity of the searching for DM particles in space. Many targets have been studied thoroughly to search for DM signals based on the Fermi-LAT data, including the Milky Way dwarf galaxies [9–15], clusters of galaxies [16–21], the center and halo of the Milky Way [22–28], the globular clusters [29] and so on. Also there were efforts to search for the monochromatic line emission from the Fermi-LAT data [30–35]. Some tentative candidates of DM signals were reported from the  $\gamma$ -ray data of the Galactic center region [23, 24] and a few ultra-faint dwarf galaxies [36, 37]. However, no consistent and conclusive evidence of DM signals can be established yet. Effective constraints on the DM model parameters can be set according to the non-detection of DM signals.

As the nearest (with a distance of  $785 \pm 25$  kpc [38]) large galaxy, the Andromeda galaxy (M31) is also a potentially good target for DM searches [16, 39–41]. The location of M31 is away from the Galactic plane ( $b \approx -22^\circ$ ) which will be less polluted by the strong Galactic foreground emission. Although it is relatively faint, M31 has been detected at  $\gamma$ -ray band by the Fermi-LAT [42–44]. Its  $\gamma$ -ray spectrum and luminosity are consistent with predictions from cosmic ray collisions with the interstellar medium (ISM), just as those established for

the Milky Way. Taking the detected flux as the upper limit on the DM induced  $\gamma$ -ray emission from M31, conservative limits on the DM annihilation cross section or decay lifetime were derived [16, 42].

In this work, we use the 7.5 year data of the Fermi-LAT to improve the sensitivity of searches for DM annihilation signal in M31. The prediction of DM annihilation induced  $\gamma$ -ray flux depends on the detailed structure of the DM distribution. Currently the knowledge about the DM distribution, especially at small scales, largely relies on numerical simulations [45–48]. High-resolution numerical simulations show that a large population of subhalos which could extend down to very low masses exist in the main DM halo [47–49]. It was pointed out that subhalos will alter the spatial extension of the DM induced  $\gamma$ -ray signals and affect the search strategy of DM particles [50]. Therefore we will discuss different spatial distributions of the M31 halo as well as the subhalo population in this work. The spatial templates of DM annihilation induced  $\gamma$ -rays are built and implemented in the likelihood analysis of the Fermi-LAT data. Typical annihilation channels to a pair of  $b$  quarks, gauge bosons, or charged leptons will be discussed. We will also discuss the inverse Compton scattering (ICS) component from DM annihilation induced electrons/positrons. And for the first time we will include an energy dependent template of the ICS emission (i.e., a template cube) in the data analysis to take the effect of diffusion of charged particles into account.

## 2 Gamma ray flux from DM annihilation in M31

Assuming the DM particles are Majorana fermions, the  $\gamma$ -ray flux from DM annihilation as a function of energy  $E$  and direction  $\theta$  can be written as

$$\frac{d\Phi}{dEd\Omega}(\theta, E) = W(E) \times J(\theta) = \frac{\langle\sigma v\rangle}{2m_\chi^2} \frac{dN_\gamma}{dE} \times \frac{1}{4\pi} \int_{l.o.s} ds \rho_{\text{DM}}^2(r(s)). \quad (2.1)$$

where the integral is computed along the line of sight (l.o.s.),  $W(E)$  and  $J(\theta)$  represent the energy and spatial dependent parts,  $m_\chi$  is the mass of the DM particle,  $\langle\sigma v\rangle$  is the velocity weighted average pair annihilation cross section,  $dN_\gamma/dE$  is the energy spectrum of  $\gamma$ -rays for one annihilation which is computed with the Pythia simulation code [51], and  $\rho_{\text{DM}}(r)$  denotes the DM density distribution.

### 2.1 DM density profile

The expected  $\gamma$ -ray signal depends crucially on the DM density profile  $\rho_{\text{DM}}(r)$  of the halo. The universal density profile suggested by Navarro, Frenk and White (hereafter NFW) found in numerical simulations [46] is widely adopted to describe the DM density distribution in the main galactic halo

$$\rho_{\text{NFW}}(r) = \frac{\rho_s}{(r/r_s)(1+r/r_s)^2}, \quad (2.2)$$

where  $r$  is the radial distance from the halo center,  $\rho_s$  and  $r_s$  are the density normalization and scale radius respectively.

With even higher resolution of numerical simulations, the asymptotic flat Einasto (EIN) profile [52] is shown to better fit the simulation results at the central part [53, 54], which reads

$$\rho_{\text{EIN}}(r) = \rho_s \cdot \exp \left[ -\frac{2}{\alpha} \left( \left( \frac{r}{r_s} \right)^\alpha - 1 \right) \right]. \quad (2.3)$$

We should keep in mind that the density profile may have uncertainties if we extrapolate the simulation results down to very small scales. Furthermore, the above profiles were derived based on the pure DM simulations. The DM density profile may get changed when the effect of baryons are taken into account [55]. Therefore we also discuss the isothermal (ISO) density profile as a conservative example. The isothermal density profile is given by [56]

$$\rho_{\text{ISO}}(r) = \frac{\rho_s}{1 + (r/r_s)^2}. \quad (2.4)$$

The measured virial mass of M31 ranges from  $0.7 \times 10^{12}$  to  $2.1 \times 10^{12} M_\odot$  [57–62]. In this work we assume the virial mass of M31 is  $M_{\text{vir}} \approx 1.0 \times 10^{12} M_\odot$  with a virial radius of  $r_{\text{vir}} \approx 205$  kpc. These values are similar with that of our Milky Way [63]. Therefore we adopt similar profile parameters for M31 as that of the Milky Way halo. The parameters are shown in Table 1 [45, 64, 65]. Note that the normalization  $\rho_s$  is derived through normalizing the total mass to  $M_{\text{vir}}$ .

halo model	$r_s$ (kpc)	$\rho_s$ (GeV/cm <sup>3</sup> )
NFW	20	0.26
EIN	20	0.06
ISO	5	0.46

Table 1. Parameters of different density profiles of M31.

## 2.2 Substructures

Abundant subhalos are expected to form based on the structure formation scenario of cold DM particles. Since the DM annihilation rate depends on the density square of DM, the existence of subhalos can boost the annihilation signal considerably with respect to the signal from the main halo. Also the spatial distribution of subhalos differ significantly from that of the main halo [50]. Here we adopt the extracted subhalo distribution from the high resolution simulation Phoenix [50]. Extrapolating the mass of subhalos to a minimum mass of  $\sim 10^{-6} M_\odot$ , the boost factor of the DM annihilation from subhalos is [50]

$$b(M_{\text{vir}}) = L_{\text{sub}}/L_{\text{main}} = 1.6 \times 10^{-3} (M_{\text{vir}}/M_\odot)^{0.39}, \quad (2.5)$$

which is about 76.6 for a virial mass of  $M_{\text{vir}} = 10^{12} M_\odot$ . The angular distribution of the annihilation  $J$ -factor of subhalos within the virial radius is

$$\begin{aligned} J_{\text{sub}}(\theta) &= \frac{b(M_{\text{vir}})L_{\text{main}}}{4\pi d^2} \times f(\theta) \\ &= \frac{b(M_{\text{vir}})L_{\text{main}}}{4\pi d^2} \times \frac{16d^2}{\pi \ln 17 r_{\text{vir}}^2} \frac{1}{1 + (4d \sin \theta / r_{\text{vir}})^2}, \end{aligned} \quad (2.6)$$

where  $d$  is the distance of the halo center to the Earth,  $L_{\text{main}} = \int_{\text{main}} \rho_{\text{DM}}^2 dV$  is the total annihilation luminosity of the main halo.

Here we assume a “smooth” distribution of subhalos in the main halo. Such an approximation is acceptable considering the finite spatial resolution of  $\gamma$ -ray detectors. Considering the maximum subhalo with a mass of  $\sim 10^{10} M_\odot$ , its virial radius is about 40 kpc. For an NFW density profile, most of the DM annihilation occurs within a few percent of the virial

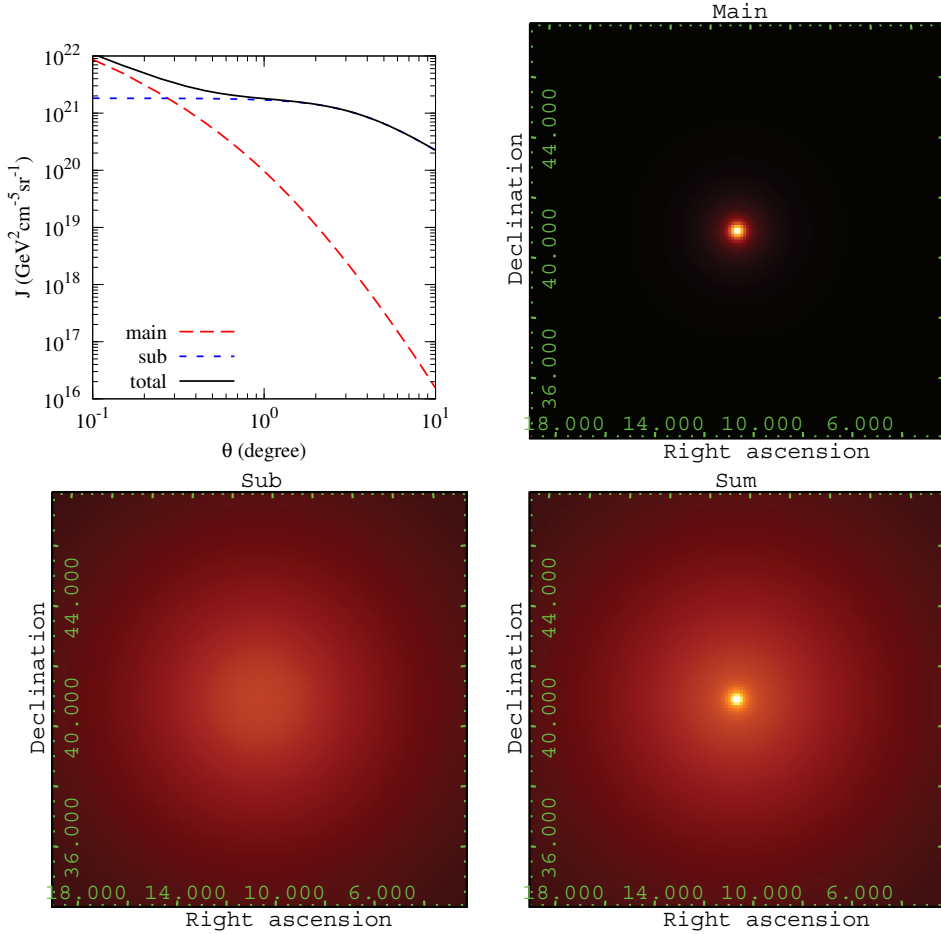


**Figure 1.** The astrophysical factor  $J$  of the DM annihilation in the main halo and subhalos. The NFW profile of the main halo is assumed. The top-left panel shows the 1-dimensional distribution, and the others are 2-dimensional skymaps in a  $14^\circ \times 14^\circ$  region centered on M31 of the main halo (top-right), subhalos (bottom-left) and the sum (bottom-right).

radius [48], which corresponds to an angular radius of  $\lesssim 0^\circ.1$  for a distance of  $\sim 800$  kpc. Given the best resolution angle of the Fermi-LAT is about  $0^\circ.1$  [8] and most of the photons from the direction of M31 have energies below  $\sim 10$  GeV, even the brightest subhalo in M31 is nearly unresolvable by the Fermi-LAT. Therefore it is reasonable to assume a “smooth” distribution of all subhalos.

The total  $J$ -factor is thus the sum of the two components:  $J_{\text{tot}}(\theta) = J_{\text{main}}(\theta) + J_{\text{sub}}(\theta)$ . Figure 1 shows the 1-dimensional (top-left panel) and 2-dimensional distributions of  $J_{\text{main}}$  (top-right),  $J_{\text{sub}}$  (bottom-left) and  $J_{\text{tot}}$  (bottom-right). The results show that the  $\gamma$ -ray flux from the main halo is highly concentrated, while the subhalo contribution is much flatter. These sky distributions will be used as spatial templates for the analysis of the Fermi-LAT data in the following.

### 3 Data analysis

The detection of  $\gamma$ -ray emission from M31 was reported in Ref. [42]. The  $\gamma$ -ray emission slightly favors (at  $1.8\sigma$  confidence level) a spatially extended source coincident with the 100  $\mu\text{m}$  far infrared image of the Improved Reprocessing of the IRAS Survey (IRIS) [66]. The best fitting spectral index is  $\Gamma \approx 2.1$  for an extended template, and  $\Gamma \approx 2.5$  for a point source assumption, respectively. Slightly different values were reported in Refs. [43, 44], probably due to different energy cuts of those analyses.

The data used in our analysis are the Pass 8 events with “SOURCE” event class of the Fermi-LAT data<sup>1</sup> recorded between 4 Aug 2008 and 1 Feb 2016. We select the events with energies between 200 MeV and 500 GeV, and apply the zenith angle cut  $\theta < 100^\circ$  to suppress the contribution from the Earth limb. We further select events when the satellite’s rocking angle is less than  $52^\circ$ . The radius of the region-of-interest (ROI) is taken as  $10^\circ$  around M31. The selected events are binned with  $0.1^\circ \times 0.1^\circ$  spatial pixels and 30 logarithmic energy bins. We employ the binned likelihood analysis method to analyze the data with the LAT Scientific Tools v10r0p5. The instrument response function (IRF) adopted is P8R2\_SOURCE\_V6. For the diffuse backgrounds we use the Galactic diffuse model `gll_iem_v06.fits` and the isotropic background spectrum `iso_P8R2_SOURCE_V6_v06.txt` as recommended by the Fermi-LAT collaboration<sup>2</sup>.

We use the likelihood tool `gtlike` to perform the analysis. The source model XML file is generated using the user contributed `make3FGLxml.py` tool<sup>3</sup> based on the 3FGL source catalog [67]. The spatial template of M31 is also adopted to be the IRIS 100  $\mu\text{m}$  far infrared image. The spectrum of M31 is modeled as a power-law function. Setting all the source parameters within the ROI and the normalizations of the two diffuse backgrounds free, we do the global fit to the data. The *Test Statistic*<sup>4</sup> (TS) value of the IRIS template is 91.5, and the fitting spectral index is  $2.3 \pm 0.1$ . We also test the point source assumption, and get  $\text{TS} = 59.9$  and  $\Gamma = 2.5 \pm 0.1$ . The spectral index for point source assumption is softer than that of the extended source assumption, which is consistent with Refs. [42–44].

To check that whether the current model describes the data well or not, we generate the TS maps of the  $5^\circ \times 5^\circ$  region centered on M31. The top-left panel of Figure 2 shows the TS map without M31 in the model, overlaid with the IRIS 100  $\mu\text{m}$  image contours (green; [66]). Strong  $\gamma$ -ray emission at the location of M31 can be seen in the TS map. The top-right panel shows the TS map with the IRIS template in the model. A point-like excess at ( $00^{\text{h}}39^{\text{m}}.8$ ,  $41^\circ52'$ ) is seen. We note that the location of this source deviates from that of the satellite galaxy M110 by about  $0^\circ.22$ , which suggests a non-M110 origin of it. We then add a new point source at this position with a power-law spectrum and re-do the fit. The overall  $-\ln \mathcal{L}$  value decreases by about 8, and the TS value of this new point source is found to be about 16 which has some degeneracy with the extended emission of M31. The residual TS map for such a model is shown by the bottom-left panel of Figure 2. No significant excess can be seen from this residual TS map.

In Ref. [44] it was claimed that halo-like (or more specifically, bubble-like) excesses exist in the direction of M31. We test this result in our analysis. We first adopt a  $0^\circ.9$  radius uniform disk [44] centered on M31 as the spatial template, and find that the goodness-of-fit

---

<sup>1</sup><http://fermi.gsfc.nasa.gov/ssc/data>

<sup>2</sup><http://fermi.gsfc.nasa.gov/ssc/data/access/lat/BackgroundModels.html>

<sup>3</sup><http://fermi.gsfc.nasa.gov/ssc/data/analysis/user/>

<sup>4</sup>Defined as  $-2 \ln(\mathcal{L}/\mathcal{L}_0)$ , where  $\mathcal{L}$  ( $\mathcal{L}_0$ ) is the likelihood of the model with (without) the target source [68].

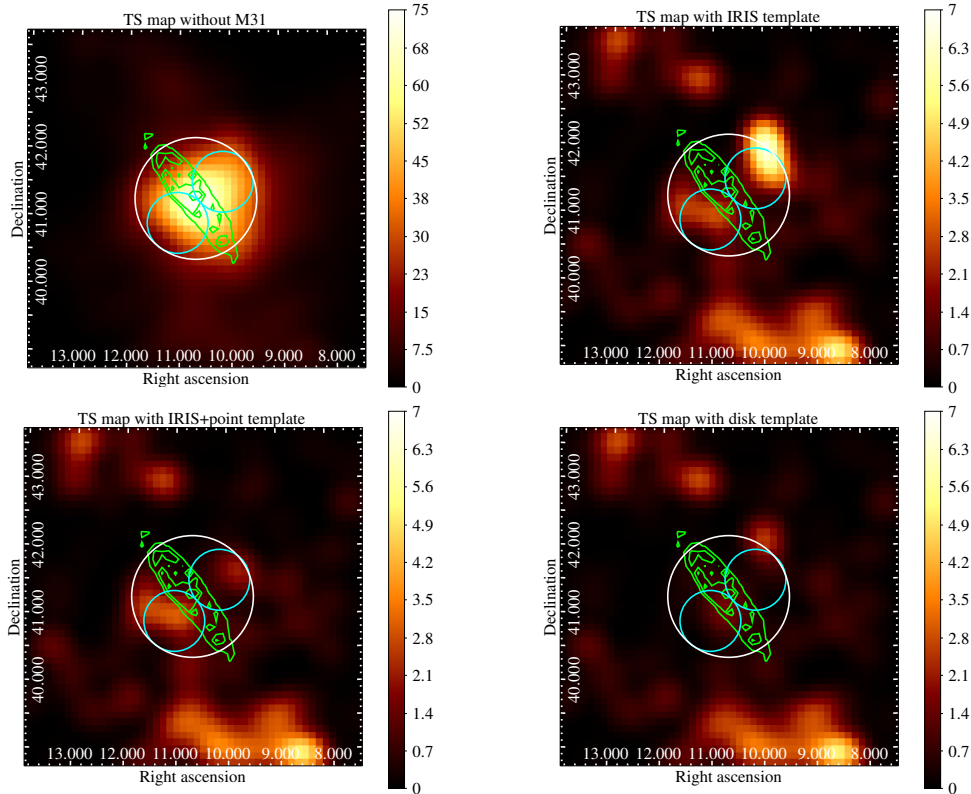


**Figure 2.** TS maps of  $5^\circ \times 5^\circ$  region centered on M31. Top-left: excluding M31 from the model; top-right: including IRIS template of M31; bottom-left: including IRIS template and an additional point source; bottom-right: including a  $0^\circ.9$  radius uniform disk template. Overlaid are the IRIS  $100 \mu\text{m}$  contours of M31 (green), a  $0^\circ.9$  radius circle (white), and two  $0^\circ.45$  radius circles (cyan) representing the bubbles adopted in Ref. [44]. The TS maps are smoothed with Gaussian kernels with  $\sigma = 0^\circ.2$ .

$(-\ln \mathcal{L})$  is comparable to that of the IRIS + point case. The residual TS map is also similar to that of the IRIS + point case, as shown by the bottom-right panel of Figure 2. Then we test the model with both the IRIS template and the  $0^\circ.9$  uniform disk (two  $0^\circ.45$  bubbles), and find a slight change of the overall goodness-of-fit (see Table 2 for a summary of the fitting results). Due to the limited spatial resolution of the Fermi-LAT data, it is difficult to draw a definite conclusion about the nature of the residual emission yet. Later we will show that, such emission would even degenerate with that from some DM annihilation models. However, as will be discussed in Sec. 4, such emission is less likely to be of DM origin. Therefore we assume the IRIS + point model as the astrophysical background in the following analysis.

To derive the spectral energy distribution (SED) of M31, we divide the data into eight energy bins from 200 MeV to 100 GeV, and use `gtlike` to fit the flux of M31 (the IRIS component) in each bin. During the fit we fix the spectral parameters of all sources to the values derived in the global fitting, and leave the normalizations of all point sources within the ROI, and the normalizations of the diffuse backgrounds free. The results are shown in Figure 3 (red). Also shown are the SED obtained in Ref. [42] based on two year data (blue). These two results are consistent with each other within statistical errors. We find that the data look similar to that from the decay of neutral pions produced by the interaction between



Template	$-\ln \mathcal{L}$	$\Delta N_{\text{dof}}$
IRIS	190463.0	—
IRIS + point	190454.9	4
$0^\circ.9$ disk <sup>a</sup>	190456.1	1
IRIS + $0^\circ.9$ disk <sup>a</sup>	190455.7	3
IRIS + two bubbles <sup>a</sup>	190453.8	3

Note: <sup>a</sup>The radius of the disk or bubbles contributes 1 to the number of degree-of-freedom.

**Table 2.** Comparison of the goodness-of-fit of various spatial templates.

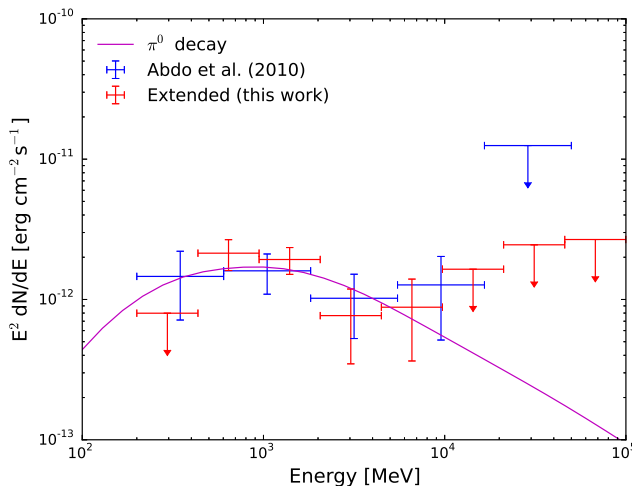


**Figure 3.** SED of M31 obtained in this work (red), compared with that reported in Ref. [42]. The solid line shows the expectation from the  $pp$ -collision-induced  $\gamma$ -ray spectrum for a proton spectrum similar to that of the Milky Way.

cosmic ray protons and gas, as shown by the solid line. Here we parameterize the proton spectrum as  $dN/dE_k \propto (1 + E_k/1.6 \text{ GeV})^{-2.8}$ , which is similar to that of the Milky Way.

## 4 Constraints on DM annihilation models

### 4.1 Prompt radiation only

Now we discuss the potential emission from the annihilation of DM. In this subsection we consider only the prompt radiation produced directly associated with the DM annihilation. We add an extended source with spatial distribution proportional to the  $J$ -factor as expected from the DM annihilation and fit to the data. During the fitting we fix the spectral parameters of all sources in the ROI to the values obtained in the global fitting described in Sec. 3, and leave the normalizations of these sources and the diffuse backgrounds, as well as the normalization of the DM component free. The energy spectrum of the DM component is calculated by Pythia, given the mass of the DM particle and the annihilation channel.

We find that in some cases the DM annihilation component degenerates with the astrophysical background emission of M31. In particular, for  $m_\chi \sim 16 \text{ GeV}$  and  $b\bar{b}$  annihilation channel, the inclusion of the DM annihilation component from the main halo gives



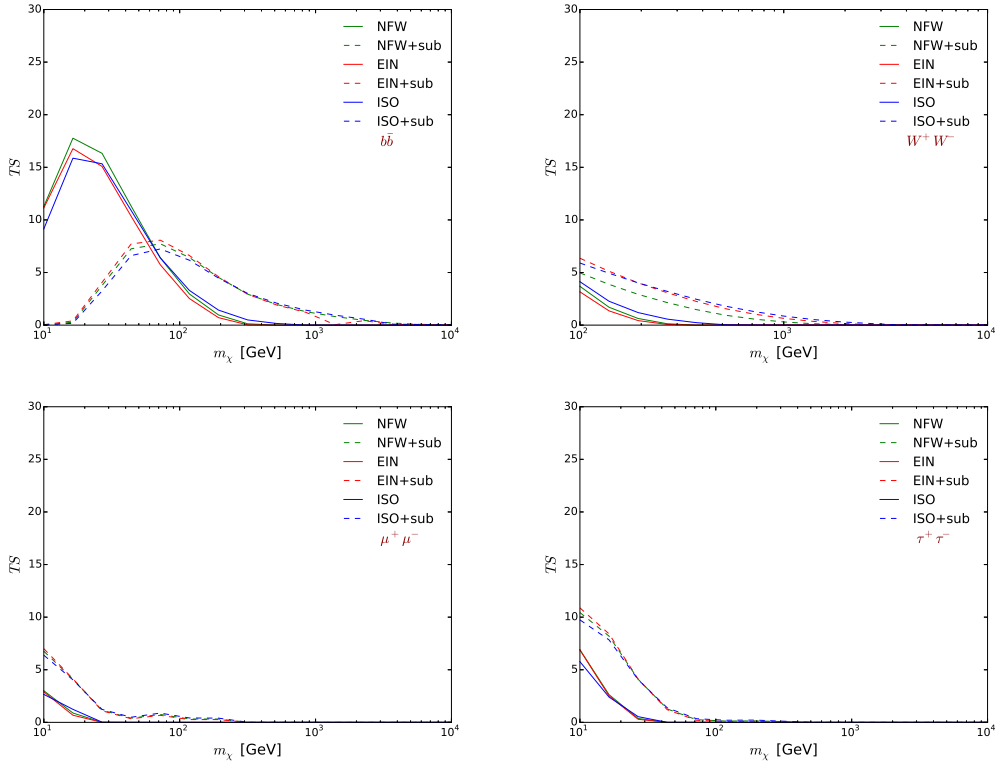


**Figure 4.** TS values of the DM component for four annihilation channels:  $b\bar{b}$  (top-left),  $W^+W^-$  (top-right),  $\mu^+\mu^-$  (bottom-left), and  $\tau^+\tau^-$  (bottom-right).

$-\ln \mathcal{L} = 190446$ . It corresponds to a TS value of the DM component of  $\sim 18$  compared with the *null* hypothesis ( $-\ln \mathcal{L}_0 = 190454.9$ ), as shown in Figure 4<sup>5</sup>. In this case the DM component also shares a large fraction of the flux of M31, resulting in a very low significance of M31 itself. However, it is unlikely that the data favor a DM component because the inferred cross section of  $\sim 10^{-25} - 10^{-24} \text{ cm}^3\text{s}^{-1}$  (see below Figure 6) is orders of magnitude higher than the constraints from the Fermi-LAT observations of dwarf spheroidal galaxies [14]. When DM subhalos are taken into account, the degeneracy is broken and the corresponding TS value of the DM component decreases significantly, which implies that the morphology of the  $\gamma$ -ray emission is not traced by the  $J_{\text{tot}}$  distribution. Therefore we assume that the excess emission from the direction of M31 has an astrophysical origin, and place upper limits on the DM model parameters instead. The degeneracy between the DM signal and the astrophysical background, however, makes these upper limits be higher, and the corresponding constraints on the DM cross section be more conservative.

The upper limits for the  $\gamma$ -ray fluxes above 100 MeV from DM annihilation of M31 for  $b\bar{b}$ ,  $W^+W^-$ ,  $\mu^+\mu^-$ , and  $\tau^+\tau^-$  channels are shown in Figure 5. The lower (higher) group in each panel represents the cases without (with) subhalos. If subhalos are not taken into account, the derived upper limits differ from each other for different assumed density profiles. The flatter the density profile, the higher the flux limit. When subhalos are included, we find that the flux upper limits are quite similar for different profiles of the smooth halo. This

<sup>5</sup>For  $W^+W^-$ ,  $\mu^+\mu^-$ , and  $\tau^+\tau^-$  channels the TS values are smaller, because the  $\gamma$ -ray spectra from these final states are harder and deviate more from the background.

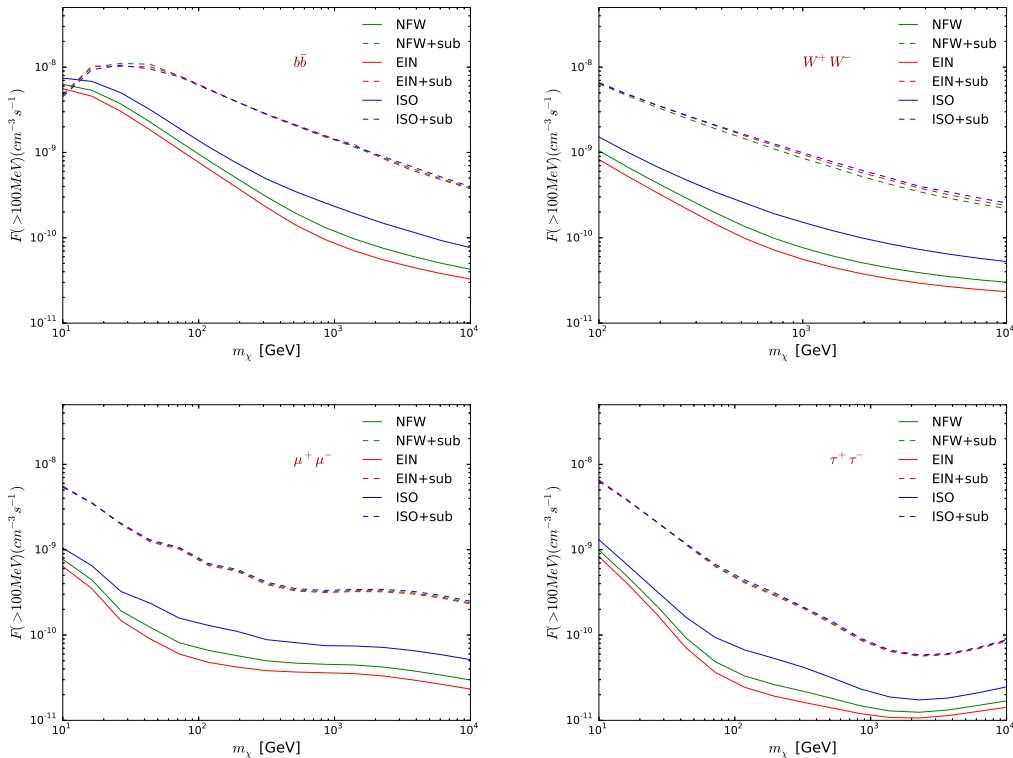


**Figure 5.** 95% upper limits of  $> 100$  MeV  $\gamma$ -ray flux of the DM annihilation component, for  $b\bar{b}$  (top-left),  $W^+W^-$  (top-right),  $\mu^+\mu^-$  (bottom-left), and  $\tau^+\tau^-$  (bottom-right) channels, respectively. See the text for details.

is because the contribution from subhalos dominate over the main halo, and we assume the same subhalo distribution (Eq. (2.6)) in this work. However, since the  $J$ -factors will be different for the three main halo profiles, we will get different constraints on the DM model parameters (see below).

The 95% upper limits on the DM annihilation cross sections are presented in Figure 6. For comparison we also show the results from the combined analysis of Fermi-LAT observations of 15 dwarf spheroidal galaxies [14]. It is shown that the constraints for NFW and EIN profiles are comparable with each other, while for ISO profile they are weaker by almost an order of magnitude. Including subhalos will improve the limits by a factor of  $\sim 10$ , although the flux limits are higher. Compared with the results from dwarf galaxies, the constraints from M31 will be generally weaker if the subhalos are not considered. If subhalos are taken into account and the density profile of the main halo is cuspy, our derived constraints are comparable to (or slightly weaker than) that from the population of dwarf spheroidal galaxies.

The lepton pair channels  $\mu^+\mu^-$  and  $\tau^+\tau^-$  are motivated by the recent observations of electron/positron excesses [5, 6, 69–71], and non-excess of antiprotons [72, 73]. In the lower two panels of Figure 6 we show the required parameter regions to fit the electron/positron excesses measured by PAMELA/Fermi-LAT/AMS-02 [74, 75]. It is shown that for  $\mu^+\mu^-$  channel the current limits from M31 can marginally constrain the  $e^+e^-$  excess favored parameter regions. For DM annihilation into  $\tau^+\tau^-$ , the model will predict too many  $\gamma$ -ray

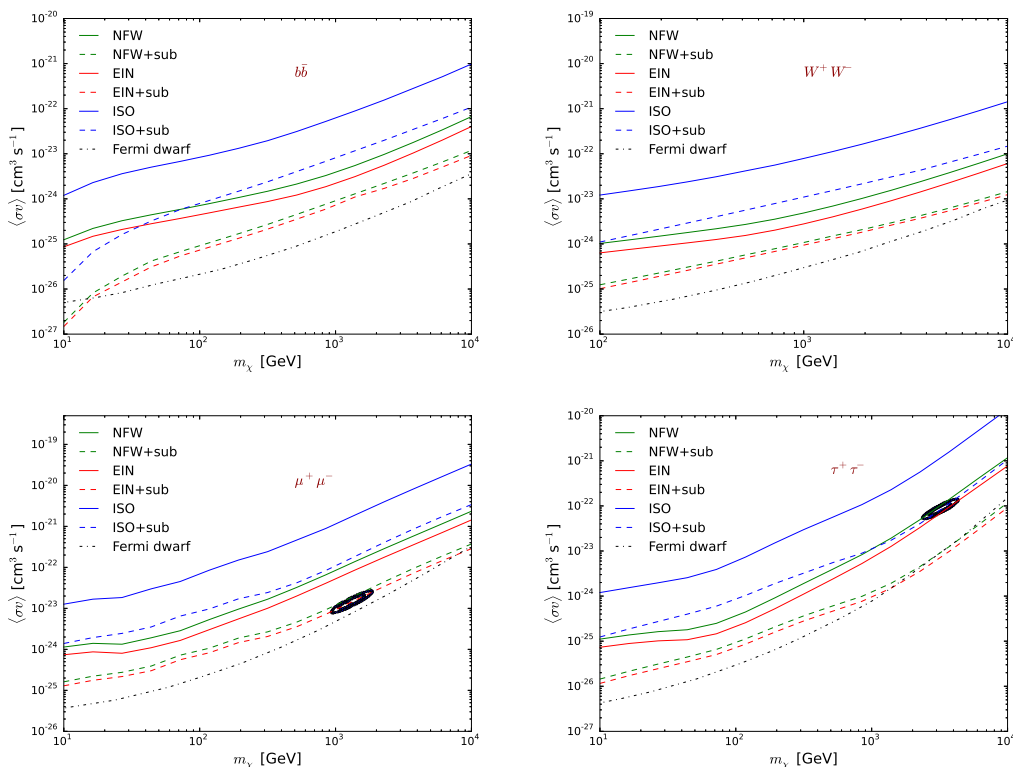


**Figure 6.** 95% confidence level constraints on DM annihilation cross section for the four annihilation channels as shown in Figure 5. For comparison, the black dot-dashed line shows the result from the combined analysis of Fermi-LAT data of 15 dwarf spheroidal galaxies [14].

photons and is in significant conflict with the Fermi-LAT observations of M31.

## 4.2 Including ICS emission

In the above discussion the ICS contribution from DM annihilation induced  $e^+e^-$  is not included. Here we discuss the effect of the ICS component. We take NFW profile and  $\mu^+\mu^-$  annihilation channel as an example. DM subhalos are not taken into account. A spherical geometry of the electron propagation in the halo of M31 is assumed. The propagation equation can be written as

$$\nabla \cdot \left[ D(E, \mathbf{r}) \nabla \frac{dn}{dE} \right] + \frac{\partial}{\partial E} \left[ b(E, \mathbf{r}) \frac{dn}{dE} \right] + Q(E, \mathbf{r}) = 0, \quad (4.1)$$

where  $dn/dE$  is the equilibrium density distribution of  $e^+e^-$ ,  $D(E, \mathbf{r})$  is the diffusion coefficient,  $b(E, \mathbf{r}) = -dE/dt$  is the absolute energy loss rate, and  $Q(E, \mathbf{r})$  is the source injection rate. We assume a homogeneous diffusion coefficient,  $D(E) = 3 \times 10^{28} (E/\text{GeV})^{1/3}$ , as that in the Milky Way. Since here we consider a large halo of M31, we neglect the interstellar radiation field from stars and dust, and only consider the cosmic microwave background (CMB) photons to calculate the cooling and ICS emission of the  $e^+e^-$ . The cooling rate is then  $b(E) = 2.5 \times 10^{-17} (E/\text{GeV})^2 \text{ GeV s}^{-1}$ .

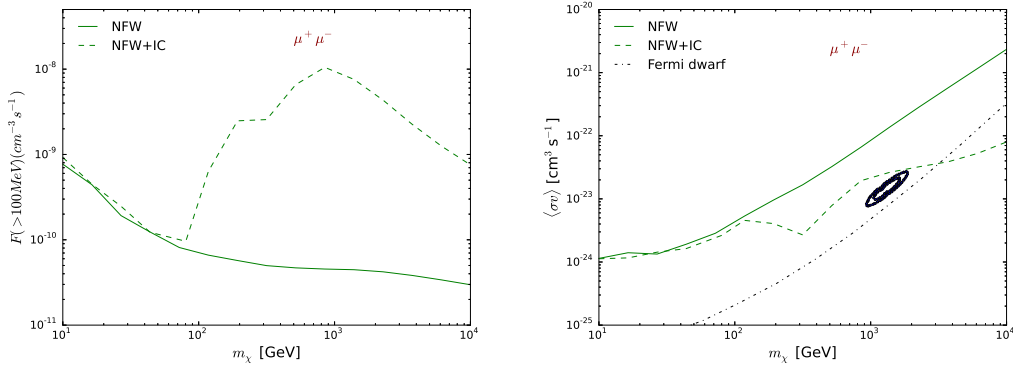


**Figure 7.** 95% confidence level upper limits of the  $> 100$  MeV  $\gamma$ -ray flux (left) and the DM annihilation cross section (right) when the ICS component is taken into account. The annihilation channel is  $\mu^+\mu^-$  and the density profile of the main halo is NFW.

The solution of Eq. (4.1) is [7]

$$\frac{dn}{dE} = \frac{1}{b(E)} \int_E^\infty dE' G(r, \Delta v) Q(E', r), \quad (4.2)$$

where

$$G(r, \Delta v) = \frac{1}{\sqrt{4\pi\Delta v}} \sum_{n=-\infty}^{+\infty} \int_0^{r_h} dr' \frac{r'}{r_n} \times \left[ \exp\left(-\frac{(r' - r_n)^2}{4\Delta v}\right) - \exp\left(-\frac{(r' + r_n)^2}{4\Delta v}\right) \right] \frac{\rho^2(r')}{\rho^2(r)}, \quad (4.3)$$

$r_h = r_{\text{vir}}$ ,  $r_n = (-1)^n r + 2nr_h$ , and  $\Delta v(E, E') = \int_E^{E'} de D(e)/b(e)$ . Given the equilibrium  $e^+e^-$  spectrum, the ICS emission at each location  $r$  can be calculated using the Klein-Nishina differential scattering cross section [76, 77].

For each mass of the DM particle, we calculate the  $\gamma$ -ray (both the ICS and the prompt radiation) emissivity as a function of photon energy  $E$  and radius  $r$ , and integrate along the l.o.s. of given direction  $\theta$ . A skymap in each energy bin can be obtained. Similar to the Galactic diffuse  $\gamma$ -ray template, we build a template cube of the DM-induced photon emission which is embedded in the model for the fitting.

The results are shown in Figure 7. The left panel shows the flux upper limits, and the right panel shows the constraints on the DM cross section. For  $m_\chi \lesssim 100$  GeV the ICS photon energies are essentially smaller than 100 MeV and the Fermi-LAT data cannot give effective constraint. For  $m_\chi > 100$  GeV the ICS component enters the Fermi-LAT energy region. The flux upper limits show a remarkable increase for  $m_\chi > 100$  GeV, possibly because, compared with the prompt radiation, the spatial distribution of the ICS emission is more extended and the spectrum is softer, which mimics the background more. Nevertheless, the constraints on  $\langle\sigma v\rangle$  are stronger than the case with only the prompt radiation, as shown in the right panel of Figure 7. For  $m_\chi \gtrsim \text{TeV}$  the constraints can improve by a factor of a few to  $\sim 10$ .

## 5 Conclusion and discussion

In this work, we analyze 7.5 year Fermi-LAT  $\gamma$ -ray data of M31 to probe the particle DM annihilation models. We confirm the results in Ref. [44] that there is residual excess from the vicinity of M31 besides the extended emission from the galactic disk as traced by the far infrared dust emission. However, the detailed morphology of the residual is not clear yet, which needs further studies with improved photon statistics and angular resolution. When adding an additional point source located at  $\sim 0^\circ.9$  away from the galaxy center, a relatively clean residual TS map is obtained. Slight improvements of the fittings are found if an extended uniform disk or two bubble-like templates are added instead of the point source. These results may imply that the dust emission template is not good enough to describe the  $\gamma$ -ray emission from M31. As we learn from the Milky Way, the diffuse  $\gamma$ -ray emission should be the convolution of the cosmic ray distribution and the gas distribution. Furthermore, the ICS emission from cosmic ray electrons will also make the  $\gamma$ -ray distribution deviate from the dust distribution. Finally, a few bright point sources such as pulsars may contribute effectively to the  $\gamma$ -ray emission of an extragalactic galaxy [78].

Using the far infrared dust template and an additional point source as the background model of M31, we search for the DM annihilation signals. We find that for  $m_\chi \sim$  a few tens of GeV and  $b\bar{b}$  annihilation channel, the DM emission from the main halo (i.e., without subhalos) degenerates with the galaxy emission significantly. If the DM annihilation from a smooth NFW/EIN halo is employed to explain the majority of the  $\gamma$ -ray emission, the required cross section is  $\sim 10^{-25} \text{ cm}^3 \text{ s}^{-1}$ , which is well above the exclusion limits from dwarf galaxy observations [14]. Therefore it is unlikely that DM annihilation dominates the  $\gamma$ -ray emission of M31.

If the subhalos are taken into account, the degeneracy is broken and more stringent constraints on the DM parameter space can be derived. For NFW and EIN profiles, the constraints are stronger by a factor of  $\sim 10$  than that for ISO profile. The most stringent constraints (for NFW or EIN profile with subhalos) set by the Fermi-LAT observations of M31 are comparable to (for leptonic channels) or slightly weaker than (for quark and gauge boson channels) that of the combined analysis of 6 year observations of 15 dwarf galaxies [14]. The parameter regions to explain the  $e^+e^-$  excesses will be excluded if the DM annihilation luminosity is enhanced by subhalos.

We also test the effect of including the ICS component from DM annihilation induced electrons/positrons. For the first time we employ an energy dependent template cube of the ICS emission in the data analysis to compute the likelihood and upper limits. The resulting constraints on  $\langle\sigma v\rangle$  are improved remarkably for  $m_\chi \gtrsim 100$  GeV.

## Acknowledgments

We thank the anonymous referee for helpful suggestions, and Eric Albin, Yi-Zhong Fan, Zhao-Qiang Shen, and Zi-Qing Xia for useful discussion. Q.Y. is supported by the National Key Program for Research and Development (No. 2016YFA0400200) and the 100 Talents program of Chinese Academy of Sciences.

## References

- [1] F. Zwicky, *Die Rotverschiebung von extragalaktischen Nebeln*, *Helvetica Physica Acta* **6** (1933) 110–127.

- [2] G. Jungman, M. Kamionkowski and K. Griest, *Supersymmetric dark matter*, *Phys. Rept.* **267** (Mar., 1996) 195–373, [[hep-ph/9506380](#)].
- [3] G. Bertone, D. Hooper and J. Silk, *Particle dark matter: evidence, candidates and constraints*, *Phys. Rept.* **405** (Jan., 2005) 279–390, [[hep-ph/0404175](#)].
- [4] D. Hooper and S. Profumo, *Dark matter and collider phenomenology of universal extra dimensions*, *Phys. Rept.* **453** (Dec., 2007) 29–115, [[hep-ph/0701197](#)].
- [5] J. Chang, J. Adams, H. Ahn, G. Bashindzhagyan, M. Christl et al., *An excess of cosmic ray electrons at energies of 300–800 GeV*, *Nature* **456** (2008) 362–365.
- [6] O. Adriani and et al., *An anomalous positron abundance in cosmic rays with energies 1.5–100 GeV*, *Nature* **458** (Apr., 2009) 607–609, [[0810.4995](#)].
- [7] S. Colafrancesco, S. Profumo and P. Ullio, *Multi-frequency analysis of neutralino dark matter annihilations in the Coma cluster*, *Astron. Astrophys.* **455** (Aug., 2006) 21–43, [[astro-ph/0507575](#)].
- [8] Fermi-LAT Collaboration, W. B. Atwood et al., *The Large Area Telescope on the Fermi Gamma-Ray Space Telescope Mission*, *Astrophys. J.* **697** (June, 2009) 1071–1102, [[0902.1089](#)].
- [9] FERMI-LAT collaboration, A. A. Abdo et al., *Observations of Milky Way Dwarf Spheroidal galaxies with the Fermi-LAT detector and constraints on Dark Matter models*, *Astrophys. J.* **712** (2010) 147–158, [[1001.4531](#)].
- [10] Fermi-LAT Collaboration, M. Ackermann et al., *Constraining Dark Matter Models from a Combined Analysis of Milky Way Satellites with the Fermi Large Area Telescope*, *Phys. Rev. Lett.* **107** (Dec., 2011) 241302, [[1108.3546](#)].
- [11] A. Geringer-Sameth and S. M. Koushiappas, *Exclusion of Canonical Weakly Interacting Massive Particles by Joint Analysis of Milky Way Dwarf Galaxies with Data from the Fermi Gamma-Ray Space Telescope*, *Phys. Rev. Lett.* **107** (Dec., 2011) 241303, [[1108.2914](#)].
- [12] Y.-L. Sming Tsai, Q. Yuan and X. Huang, *A generic method to constrain the dark matter model parameters from Fermi observations of dwarf spheroids*, *JCAP* **3** (Mar., 2013) 18, [[1212.3990](#)].
- [13] FERMI-LAT collaboration, M. Ackermann et al., *Dark matter constraints from observations of 25 Milky Way satellite galaxies with the Fermi Large Area Telescope*, *Phys. Rev.* **D89** (2014) 042001, [[1310.0828](#)].
- [14] FERMI-LAT collaboration, M. Ackermann et al., *Searching for Dark Matter Annihilation from Milky Way Dwarf Spheroidal Galaxies with Six Years of Fermi Large Area Telescope Data*, *Phys. Rev. Lett.* **115** (2015) 231301, [[1503.02641](#)].
- [15] A. Geringer-Sameth, S. M. Koushiappas and M. G. Walker, *Comprehensive search for dark matter annihilation in dwarf galaxies*, *Phys. Rev.* **D91** (2015) 083535, [[1410.2242](#)].
- [16] L. Dugger, T. E. Jeltema and S. Profumo, *Constraints on decaying dark matter from Fermi observations of nearby galaxies and clusters*, *JCAP* **12** (Dec., 2010) 15, [[1009.5988](#)].
- [17] Q. Yuan, P.-F. Yin, X.-J. Bi, X.-M. Zhang and S.-H. Zhu, *Gamma rays and neutrinos from dark matter annihilation in galaxy clusters*, *Phys. Rev. D* **82** (July, 2010) 023506, [[1002.0197](#)].
- [18] Fermi LAT Collaboration, M. Ackermann and et al., *Constraints on dark matter annihilation in clusters of galaxies with the Fermi large area telescope*, *JCAP* **5** (May, 2010) 25, [[1002.2239](#)].
- [19] X. Huang, G. Vertongen and C. Weniger, *Probing dark matter decay and annihilation with Fermi LAT observations of nearby galaxy clusters*, *JCAP* **1** (Jan., 2012) 42, [[1110.1529](#)].
- [20] C. Combet, D. Maurin, E. Nezri, E. Pointecouteau, J. A. Hinton and R. White, *Decaying dark matter: Stacking analysis of galaxy clusters to improve on current limits*, *Phys. Rev. D* **85** (Mar., 2012) 063517, [[1203.1164](#)].

- [21] J. Han, C. S. Frenk, V. R. Eke, L. Gao, S. D. M. White, A. Boyarsky et al., *Constraining Extended Gamma-ray Emission from Galaxy Clusters*, *Mon. Not. Roy. Astron. Soc.* **427** (2012) 1651–1665, [[1207.6749](#)].
- [22] J. Ellis, K. A. Olive and V. C. Spanos, *Galactic-centre gamma rays in CMSSM dark matter scenarios*, *JCAP* **10** (Oct., 2011) 24, [[1106.0768](#)].
- [23] D. Hooper and L. Goodenough, *Dark matter annihilation in the Galactic Center as seen by the Fermi Gamma Ray Space Telescope*, *Physics Letters B* **697** (Mar., 2011) 412–428, [[1010.2752](#)].
- [24] D. Hooper and T. Linden, *Origin of the gamma rays from the Galactic Center*, *Phys. Rev. D* **84** (Dec., 2011) 123005, [[1110.0006](#)].
- [25] K. N. Abazajian and M. Kaplinghat, *Detection of a gamma-ray source in the Galactic Center consistent with extended emission from dark matter annihilation and concentrated astrophysical emission*, *Phys. Rev. D* **86** (Oct., 2012) 083511, [[1207.6047](#)].
- [26] M. Ackermann, M. Ajello, W. B. Atwood, L. Baldini, G. Barbiellini, D. Bastieri et al., *Constraints on the Galactic Halo Dark Matter from Fermi-LAT Diffuse Measurements*, *Astrophys. J.* **761** (Dec., 2012) 91, [[1205.6474](#)].
- [27] X. Huang, Q. Yuan, P.-F. Yin, X.-J. Bi and X. Chen, *Constraints on the dark matter annihilation scenario of Fermi 130 GeV gamma-ray line emission by continuous gamma-rays, Milky Way halo, galaxy clusters and dwarf galaxies observations*, *JCAP* **11** (Nov., 2012) 48, [[1208.0267](#)].
- [28] D. Hooper, C. Kelso and F. S. Queiroz, *Stringent constraints on the dark matter annihilation cross section from the region of the Galactic Center*, *Astroparticle Physics* **46** (June, 2013) 55–70, [[1209.3015](#)].
- [29] L. Feng, Q. Yuan, P.-F. Yin, X.-J. Bi and M. Li, *Search for dark matter signals with Fermi-LAT observation of globular clusters NGC 6388 and M 15*, *JCAP* **4** (Apr., 2012) 30, [[1112.2438](#)].
- [30] A. Abdo, M. Ackermann, M. Ajello, W. Atwood, L. Baldini et al., *Fermi Large Area Telescope Search for Photon Lines from 30 to 200 GeV and Dark Matter Implications*, *Physical Review Letters* **104** (Mar., 2010) 091302, [[1001.4836](#)].
- [31] T. Bringmann, X. Huang, A. Ibarra, S. Vogl and C. Weniger, *Fermi LAT search for internal bremsstrahlung signatures from dark matter annihilation*, *JCAP* **7** (July, 2012) 54, [[1203.1312](#)].
- [32] C. Weniger, *A tentative gamma-ray line from Dark Matter annihilation at the Fermi Large Area Telescope*, *JCAP* **8** (Aug., 2012) 7, [[1204.2797](#)].
- [33] M. Ackermann et al., *Search for gamma-ray spectral lines with the Fermi Large Area Telescope and dark matter implications*, *Phys. Rev. D* **88** (Oct., 2013) 082002.
- [34] FERMI-LAT collaboration, M. Ackermann et al., *Updated search for spectral lines from Galactic dark matter interactions with pass 8 data from the Fermi Large Area Telescope*, *Phys. Rev.* **D91** (2015) 122002, [[1506.00013](#)].
- [35] Y.-F. Liang, Z.-Q. Shen, X. Li, Y.-Z. Fan, X. Huang, L. Feng et al., *Search for gamma-ray line feature from a group of nearby Galaxy clusters with Fermi LAT Pass 8 data*, *Phys. Rev.* **D93** (2016) 103525, [[1602.06527](#)].
- [36] A. Geringer-Sameth, M. G. Walker, S. M. Koushiappas, S. E. Kopusov, V. Belokurov, G. Torrealba et al., *Indication of Gamma-ray Emission from the Newly Discovered Dwarf Galaxy Reticulum II*, *Phys. Rev. Lett.* **115** (2015) 081101, [[1503.02320](#)].
- [37] S. Li, Y.-F. Liang, K.-K. Duan, Z.-Q. Shen, X. Huang, X. Li et al., *Search for gamma-ray emission from eight dwarf spheroidal galaxy candidates discovered in Year Two of Dark Energy Survey with Fermi-LAT data*, *Phys. Rev.* **D93** (2016) 043518, [[1511.09252](#)].



- [38] E. Corbelli, S. Lorenzoni, R. Walterbos, R. Braun and D. Thilker, *A wide-field H I mosaic of Messier 31. II. The disk warp, rotation, and the dark matter halo*, *Astron. Astrophys.* **511** (Feb., 2010) A89, [[0912.4133](#)].
- [39] A. Falvard, E. Giraud, A. Jacholkowska, J. Lavalle, E. Nuss, F. Piron et al., *Supersymmetric dark matter in M31: can one see neutralino annihilation with CELESTE?*, *Astroparticle Physics* **20** (Jan., 2004) 467–484, [[astro-ph/0210184](#)].
- [40] C. R. Watson, Z. Li and N. K. Polley, *Constraining sterile neutrino warm dark matter with Chandra observations of the Andromeda galaxy*, *JCAP* **3** (Mar., 2012) 18, [[1111.4217](#)].
- [41] A. E. Egorov and E. Pierpaoli, *Constraints on dark matter annihilation by radio observations of M31*, *Phys. Rev. D* **88** (July, 2013) 023504, [[1304.0517](#)].
- [42] A. A. Abdo, M. Ackermann, M. Ajello et al., *Fermi Large Area Telescope observations of Local Group galaxies: detection of M 31 and search for M 33*, *Astron. Astrophys.* **523** (Nov., 2010) L2, [[1012.1952](#)].
- [43] VERITAS collaboration, R. Bird, *VERITAS Observations Of M 31 (The Andromeda Galaxy)*, in *Proceedings, 34th International Cosmic Ray Conference (ICRC 2015)*, 2015. [1508.07195](#).
- [44] M. S. Pshirkov, V. V. Vasiliev and K. A. Postnov, *Evidence of Fermi bubbles around M31*, *Mon. Not. Roy. Astron. Soc.* **459** (June, 2016) L76–L80, [[1603.07245](#)].
- [45] J. F. Navarro, C. S. Frenk and S. D. M. White, *The Structure of Cold Dark Matter Halos*, *Astrophys. J.* **462** (May, 1996) 563, [[astro-ph/9508025](#)].
- [46] J. F. Navarro, C. S. Frenk and S. D. M. White, *A Universal Density Profile from Hierarchical Clustering*, *Astrophys. J.* **490** (Dec., 1997) 493, [[astro-ph/9611107](#)].
- [47] J. Diemand, M. Kuhlen, P. Madau, M. Zemp, B. Moore, D. Potter et al., *Clumps and streams in the local dark matter distribution*, *Nature* **454** (Aug., 2008) 735–738, [[0805.1244](#)].
- [48] V. Springel, S. D. M. White, C. S. Frenk, J. F. Navarro, A. Jenkins et al., *Prospects for detecting supersymmetric dark matter in the Galactic halo*, *Nature* **456** (Nov., 2008) 73–76, [[0809.0894](#)].
- [49] V. Springel, J. Wang, M. Vogelsberger, A. Ludlow, A. Jenkins, A. Helmi et al., *The Aquarius Project: the subhaloes of galactic haloes*, *Mon. Not. Roy. Astron. Soc.* **391** (Dec., 2008) 1685–1711, [[0809.0898](#)].
- [50] L. Gao, C. S. Frenk, A. Jenkins, V. Springel and S. D. M. White, *Where will supersymmetric dark matter first be seen?*, *Mon. Not. Roy. Astron. Soc.* **419** (Jan., 2012) 1721–1726, [[1107.1916](#)].
- [51] T. Sjöstrand, S. Mrenna and P. Skands, *PYTHIA 6.4 physics and manual*, *Journal of High Energy Physics* **5** (May, 2006) 26, [[hep-ph/0603175](#)].
- [52] J. Einasto, *On the Construction of a Composite Model for the Galaxy and on the Determination of the System of Galactic Parameters*, *Trudy Astrofizicheskogo Instituta Alma-Ata* **5** (1965) 87–100.
- [53] J. F. Navarro, E. Hayashi, C. Power, A. R. Jenkins, C. S. Frenk, S. D. M. White et al., *The inner structure of  $\Lambda$ CDM haloes - III. Universality and asymptotic slopes*, *Mon. Not. Roy. Astron. Soc.* **349** (Apr., 2004) 1039–1051, [[astro-ph/0311231](#)].
- [54] J. F. Navarro, A. Ludlow, V. Springel, J. Wang, M. Vogelsberger, S. D. M. White et al., *The diversity and similarity of simulated cold dark matter haloes*, *Mon. Not. Roy. Astron. Soc.* **402** (Feb., 2010) 21–34, [[0810.1522](#)].
- [55] A. R. Duffy, J. Schaye, S. T. Kay, C. Dalla Vecchia, R. A. Battye and C. M. Booth, *Impact of baryon physics on dark matter structures: a detailed simulation study of halo density profiles*, *Mon. Not. Roy. Astron. Soc.* **405** (July, 2010) 2161–2178, [[1001.3447](#)].

- [56] J. N. Bahcall and R. M. Soneira, *The universe at faint magnitudes. I - Models for the galaxy and the predicted star counts*, *Astrophys. J. Suppl.* **44** (Sept., 1980) 73–110.
- [57] M. A. Fardal, M. D. Weinberg, A. Babul et al., *Inferring the Andromeda Galaxy’s mass from its giant southern stream with Bayesian simulation sampling*, *Mon. Not. Roy. Astron. Soc.* **434** (Oct., 2013) 2779–2802, [[1307.3219](#)].
- [58] N. W. Evans, M. I. Wilkinson, P. Guhathakurta, E. K. Grebel and S. S. Vogt, *Dynamical Mass Estimates for the Halo of M31 from Keck Spectroscopy*, *Astrophys. J. Lett.* **540** (Sept., 2000) L9–L12, [[astro-ph/0008155](#)].
- [59] L. M. Widrow, K. M. Perrett and S. H. Suyu, *Disk-Bulge-Halo Models for the Andromeda Galaxy*, *Astrophys. J.* **588** (May, 2003) 311–325, [[astro-ph/0301144](#)].
- [60] R. Ibata, S. Chapman, A. M. N. Ferguson, G. Lewis, M. Irwin and N. Tanvir, *On the Accretion Origin of a Vast Extended Stellar Disk around the Andromeda Galaxy*, *Astrophys. J.* **634** (Nov., 2005) 287–313, [[astro-ph/0504164](#)].
- [61] M. S. Seigar, A. J. Barth and J. S. Bullock, *A revised  $\Lambda$  CDM mass model for the Andromeda Galaxy*, *Mon. Not. Roy. Astron. Soc.* **389** (Oct., 2008) 1911–1923, [[astro-ph/0612228](#)].
- [62] L. L. Watkins, N. W. Evans and J. H. An, *The masses of the Milky Way and Andromeda galaxies*, *Mon. Not. Roy. Astron. Soc.* **406** (July, 2010) 264–278, [[1002.4565](#)].
- [63] X. X. Xue, H. W. Rix, G. Zhao et al., *The Milky Way’s Circular Velocity Curve to 60 kpc and an Estimate of the Dark Matter Halo Mass from the Kinematics of  $\sim 2400$  SDSS Blue Horizontal-Branch Stars*, *Astrophys. J.* **684** (Sept., 2008) 1143–1158, [[0801.1232](#)].
- [64] G. Bertone, M. Cirelli, A. Strumia and M. Taoso, *Gamma-ray and radio tests of the  $e$  excess from DM annihilations*, *JCAP* **3** (Mar., 2009) 9, [[0811.3744](#)].
- [65] D. Merritt, A. W. Graham, B. Moore, J. Diemand and B. Terzić, *Empirical Models for Dark Matter Halos. I. Nonparametric Construction of Density Profiles and Comparison with Parametric Models*, *Astron. J.* **132** (Dec., 2006) 2685–2700, [[astro-ph/0509417](#)].
- [66] M.-A. Miville-Deschênes and G. Lagache, *IRIS: A New Generation of IRAS Maps*, *Astrophys. J. Suppl.* **157** (Apr., 2005) 302–323, [[astro-ph/0412216](#)].
- [67] FERMI-LAT collaboration, F. Acero et al., *Fermi Large Area Telescope Third Source Catalog*, [1501.02003](#).
- [68] J. R. Mattox, D. L. Bertsch, J. Chiang et al., *The Likelihood Analysis of EGRET Data*, *Astrophys. J.* **461** (Apr., 1996) 396.
- [69] F. Aharonian, A. G. Akhperjanian, G. Anton and et al., *Probing the ATIC peak in the cosmic-ray electron spectrum with H.E.S.S.*, *Astron. Astrophys.* **508** (Dec., 2009) 561–564, [[0905.0105](#)].
- [70] A. A. Abdo, M. Ackermann, M. Ajello and et al., *Measurement of the Cosmic Ray  $e^+ + e^-$  Spectrum from 20GeV to 1TeV with the Fermi Large Area Telescope*, *Physical Review Letters* **102** (May, 2009) 181101, [[0905.0025](#)].
- [71] AMS-02 collaboration, M. Aguilar, G. Alberti, B. Alpat and et al., *First result from the alpha magnetic spectrometer on the international space station: Precision measurement of the positron fraction in primary cosmic rays of 0.5–350 gev*, *Phys. Rev. Lett.* **110** (Apr., 2013) 141102.
- [72] O. Adriani, G. C. Barbarino, G. A. Bazilevskaya and et al., *New Measurement of the Antiproton-to-Proton Flux Ratio up to 100 GeV in the Cosmic Radiation*, *Physical Review Letters* **102** (Feb., 2009) 051101, [[0810.4994](#)].
- [73] O. Adriani, G. C. Barbarino, G. A. Bazilevskaya and et al., *PAMELA Results on the*

*Cosmic-Ray Antiproton Flux from 60 MeV to 180 GeV in Kinetic Energy*,  
*Physical Review Letters* **105** (Sept., 2010) 121101, [[1007.0821](#)].

- [74] Q. Yuan and X.-J. Bi, *Reconcile the AMS-02 positron fraction and Fermi-LAT/HESS total  $e$  spectra by the primary electron spectrum hardening*, *Physics Letters B* **727** (Nov., 2013) 1–7, [[1304.2687](#)].
- [75] Q. Yuan and X.-J. Bi, *Systematic study of the uncertainties in fitting the cosmic positron data by AMS-02*, *JCAP* **1503** (2015) 033, [[1408.2424](#)].
- [76] G. R. Blumenthal and R. J. Gould, *Bremsstrahlung, synchrotron radiation, and compton scattering of high-energy electrons traversing dilute gases*, *Rev. Mod. Phys.* **42** (1970) 237–270.
- [77] J. Zhang, Q. Yuan and X.-J. Bi, *Galactic Diffuse Gamma Rays—Recalculation Based on New Measurements of the Cosmic Electron Spectrum*, *Astrophys. J.* **720** (Sept., 2010) 9–19, [[0908.1236](#)].
- [78] FERMI-LAT collaboration, M. Ackermann et al., *An extremely bright gamma-ray pulsar in the Large Magellanic Cloud*, *Science* **350** (2015) 801–805.